Figure S1

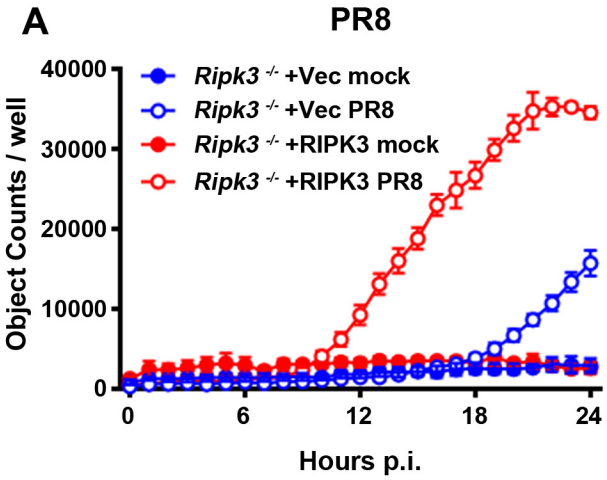

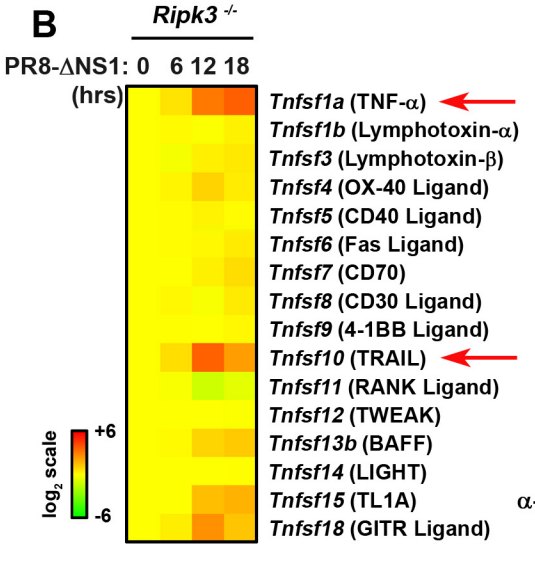

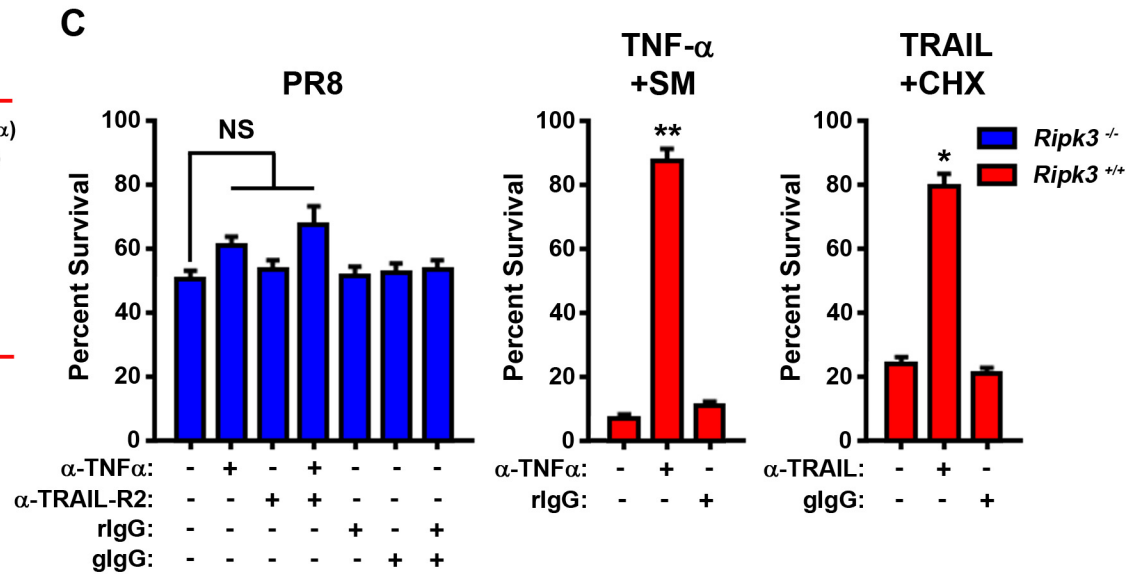

Supplementary Figure 1, related to Fig. 1. Role of TNF-α and TRAIL in IAV-activated RIPK3-independent apoptosis. (A) Reconstitution of *ripk3*$^{-/-}$ MEFs with full-length murine RIPK3 restores susceptibility to IAV-induced cell death. Immortalized *ripk3*$^{-/-}$ MEFs were retrovirally reconstituted with full-length wild-type murine RIPK3, or with a control vector (Vec), infected with PR8 (m.o.i.=5) and examined for viability by Sytox Green uptake on an Incucyte Kinetic Live Cell Imaging system. Sytox Green positive (dead) cells were expressed as object counts per well. **(B)** DNA microarray analysis profiles expression patterns of TNF superfamily members in IAV-infected *ripk3*$^{-/-}$ MEFs. For this study, we used the PR8-ΔNS1 mutant, to avoid NS1-mediated suppression of RLR responses and allow full expression of the IAV-activated transcriptome in MEFs. From this analysis, we identified only genes encoding TNF-α and TRAIL as induced > 4-fold by infection (red arrows). These data have been deposited into GEO; Series Number GSE80740. **(C)** *Ripk3*$^{-/-}$ MEFs were infected with PR8 (m.o.i.=2) in the presence or absence of neutralizing antibodies to murine TNF-α (5μg/ml) or TRAIL-R2 (10μg/ml), and viability was determined 36 h.p.i. Equivalent amounts of rabbit (rIgG) and goat (gIgG) immunoglobulins were used as controls. At these doses, anti-TNF-α and anti-TRAIL-R2 antibodies were able to robustly protect against apoptosis activated by the combinations of TNF-α (0.5ng/mL) and SMAC mimetic (5μM), or TRAIL (2μg/ml) and cycloxehimide (CHX, 250ng/ml), respectively. Error bars represent mean +/- S.D. NS = not significant; * p <0.05; ** p <0.005.

Figure S2

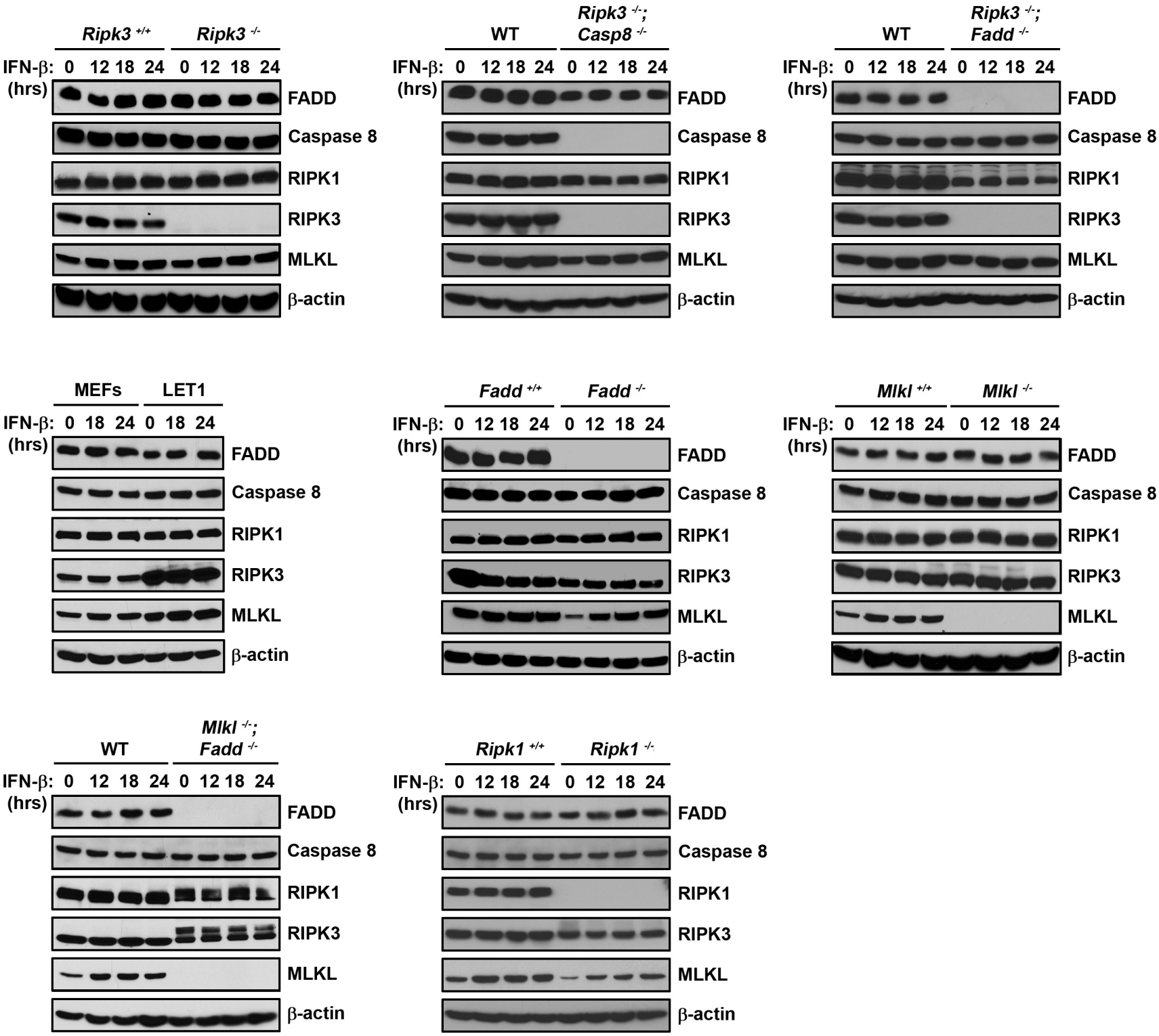
Ripk3 +/+
Ripk3 -/-
WT
Ripk3 -/-; Casp8 -/-
WT
Ripk3 -/-; Fadd -/-
MEFs
LET1
Fadd +/+
Fadd -/-
Mlkl +/+
Mlkl -/-
WT
Mlkl -/-; Fadd -/-
Ripk1 +/+
Ripk1 -/-
IFN-β: 0 12 18 24 0 12 18 24
IFN-β: 0 18 24 0 18 24
(hrs)
FADD
Caspase 8
RIPK1
RIPK3
MLKL
β-actin

Supplementary Figure 2, related to Figs. 1, 4, and 5. Levels of effector proteins in cells used in this study. Levels of key cell death effector proteins were examined in the indicated murine cell lines by immunoblot analysis following treatment with mIFN-β (1000 U/ml) for up to 24 h.

Figure S3

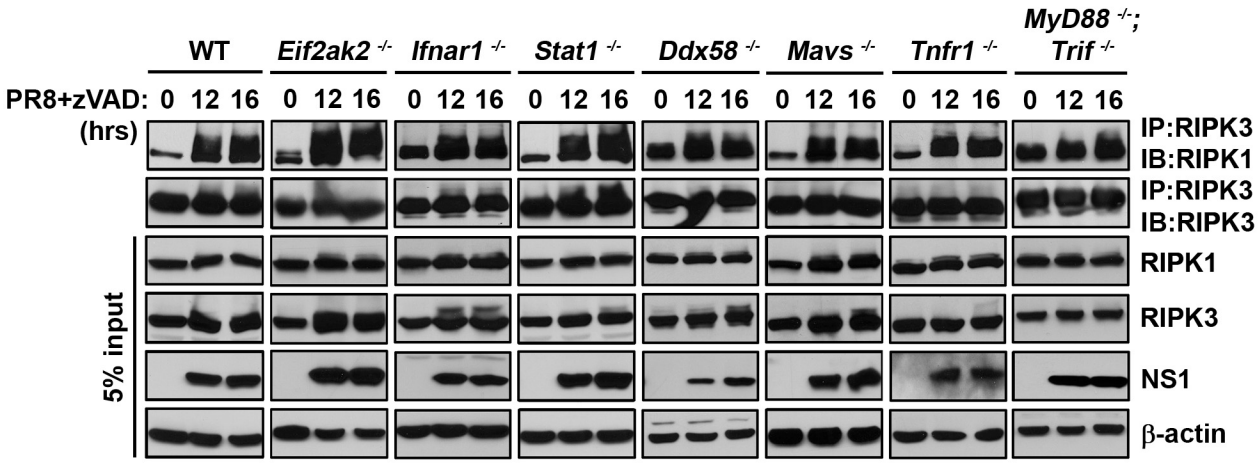

Supplementary Figure 3, related to Fig. 2. IAV-induced necrosome formation is independent of type I IFNs, TNF-α, or known RNA sensing pathways. RIPK3-RIPK1 necrosome formation was evaluated on lysates from the indicated PR8-infected wild-type or knock-out MEFs. PR8 (m.o.i.=2) in the presence of zVAD (25μM) was used to stimulate necrosome formation.

Figure S4

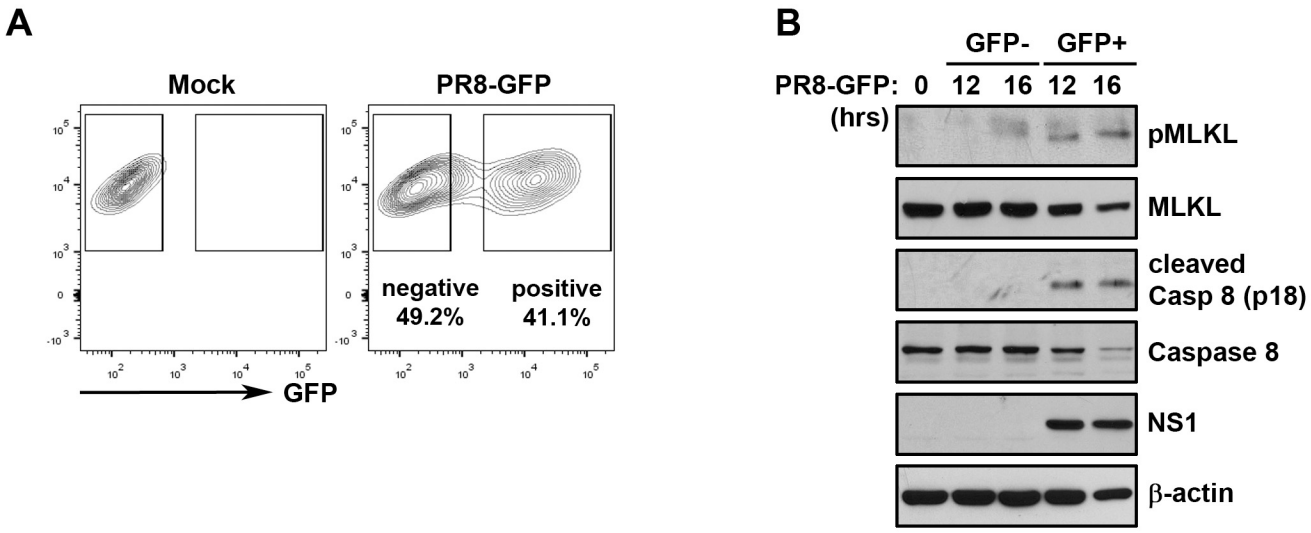

Supplementary Figure 4, related to Fig. 3. Activation of apoptosis and necroptosis is intrinsic to the IAV-infected cell. (A) Wild-type MEFs were infected with PR8-GFP (m.o.i.=2) for 18 h and sorted by GFP-positive and GFP-negative populations, representing cells harboring actively-replicating virus and cells without detectable virus replication, respectively. **(B)** GFP-positive and GFP-negative cells were examined for phosphorylation of MLKL and cleavage of caspase 8 by immunoblot analysis.

Figure S5

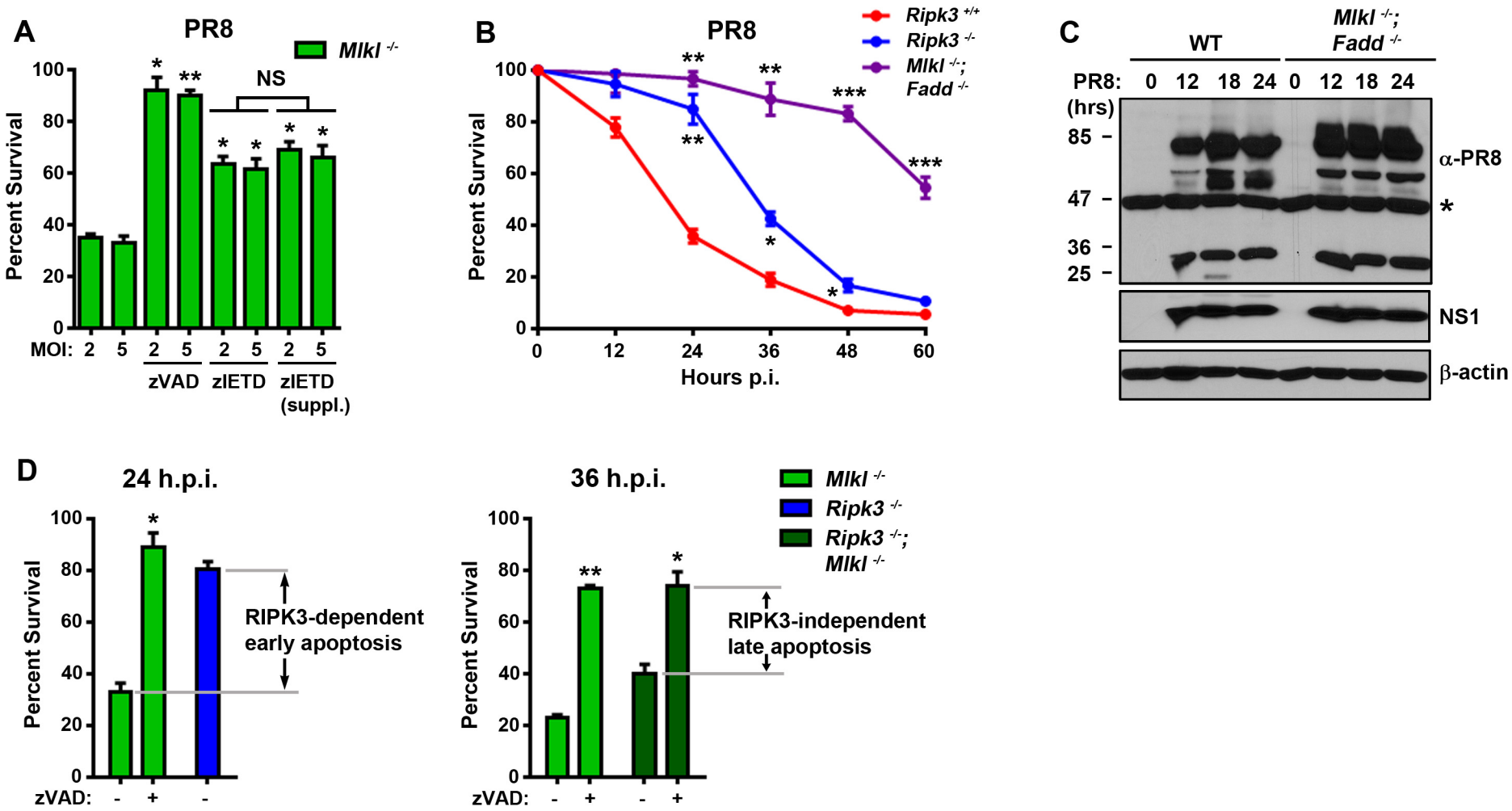

Supplementary Figure 5, related to Fig. 4. IAV activates both RIPK3-dependent early apoptosis and RIPK3-independent late apoptosis in MLKL-deficient cells. (A) zIETD is a weaker inhibitor of IAV-activated apoptosis than zVAD. *Mlkl*$^{-/-}$ MEFs were infected with PR8 in the presence or absence of zVAD (50μM), zIETD (50μM) added once, or zIETD added once and supplemented at 12 h.p.i. (two last bars), and cell viability was determined 24 h.p.i. **(B)** Kinetics of cell death after PR8 (m.o.i.=5) infection of *ripk3*$^{+/+}$, *ripk3*$^{-/-}$, and *mlkl*$^{-/-}$*fadd*$^{-/-}$ double knock-out MEFs. **(C)** Wild type (*ripk3*$^{+/+}$) and *mlkl*$^{-/-}$*fadd*$^{-/-}$ double-knockout MEFs infected with PR8 (m.o.i.=5) for the indicated times and examined for virus replication by immunoblotting with antiserum to PR8 or antibodies to NS1. A non-specific band detected in uninfected lysates by the anti-PR8 antiserum is indicated with an asterisk (*). Molecular weights (in kDa) are shown to the left. **(D)** *Mlkl*$^{-/-}$, *ripk3*$^{-/-}$, and *ripk3*$^{-/-}$*mlkl*$^{-/-}$ MEFs were infected with PR8 (m.o.i.=5) in the presence or absence of zVAD (50μM) and cell viability was determined at 24 and 36 h.p.i., to evaluate RIPK3-dependent early apoptosis and RIPK3-independent late apoptosis, respectively. Both early and late apoptosis proceed normally in cells with MLKL-deficiency. Error bars represent mean +/- S.D. NS = not significant; * p <0.05; ** p <0.005; ***p <0.0005.

Figure S6

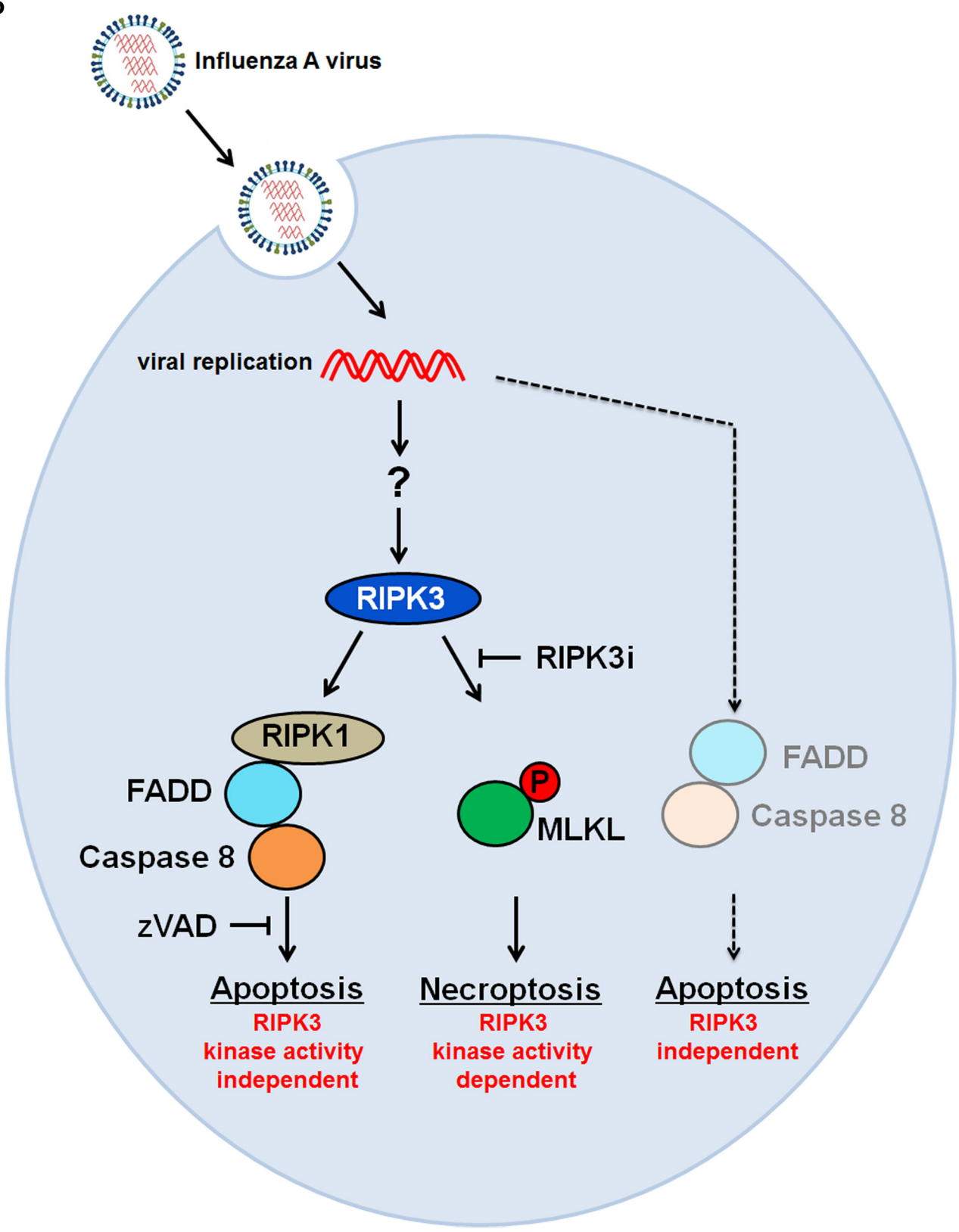

Supplementary Figure 6, related to Figs. 1, 2, 3, 4, 5 and 6. Schematic of RIPK3-dependent and -independent cell death pathways activated by IAV. Replicating IAV activates RIPK3 by an unknown mechanism. Once activated, RIPK3 initiates two parallel pathways of cell death, one proceeding via MLKL that culminates in necroptosis, and a second via RIPK1, FADD, and caspase 8 resulting in apoptosis. The MLKL-dependent necroptosis arm requires the kinase activity of RIPK3, whereas the apoptosis axis does not. IAV infection also activates a dealayed RIPK3-independent pathway of FADD/caspase 8-mediated apoptosis.